PROCEEDINGS OF SPIE

SPIEDigitalLibrary.org/conference-proceedings-of-spie

Integrated rare-Earth doped mode-locked lasers on a CMOS platform

Franz X. Kärtner, Patrick T. Callahan, Katia Shtyrkova, Nanxi Li, Neetesh Singh, et al.

Franz X. Kärtner, Patrick T. Callahan, Katia Shtyrkova, Nanxi Li, Neetesh Singh, Ming Xin, Ravi Koustuban, Jelena Notaros, E. Salih Magden, Diedrik Vermeulen, Erich P. Ippen, Michael R. Watts, "Integrated rare-Earth doped mode-locked lasers on a CMOS platform," Proc. SPIE 10686, Silicon Photonics: From Fundamental Research to Manufacturing, 106860F (30 May 2018); doi: 10.1117/12.2318010

SPIE.

Event: SPIE Photonics Europe, 2018, Strasbourg, France

Downloaded From: https://www.spiedigitallibrary.org/conference-proceedings-of-spie on 6/18/2018 Terms of Use: https://www.spiedigitallibrary.org/terms-of-use

Integrated Rare-Earth Doped Mode-Locked Lasers on a CMOS Platform

Franz X. Kärtner[a,b], Patrick T. Callahan[a], Katia Shtyrkova[a]*, Nanxi Li[a,c], Neetesh Singh[a], Ming Xin[a,b], Ravi Koustuban[a], Jelena Notaros[a], E. Salih Magden[a], Diedrik Vermeulen[a], Erich P. Ippen[a], and Michael R. Watts[a]

[a]Research Laboratory of Electronics, Massachusetts Institute of Technology, 77 Massachusetts Avenue, Cambridge, MA 02139, USA
[b]DESY - Center for Free Electron Laser Science and University of Hamburg, Notkestrasse 85, 22607 Hamburg, Germany
[c]John A. Paulson School of Engineering and Applied Science, 29 Oxford Street, Harvard University, Cambridge, MA 02138, USA

ABSTRACT

Mode-locked lasers provide extremely low jitter optical pulse trains for a number of applications ranging from sampling of RF-signals and optical frequency combs to microwave and optical signal synthesis. Integrated versions have the advantage of high reliability, low cost and compact. Here, we describe a fully integrated mode-locked laser architecture on a CMOS platform that utilizes rare-earth doped gain media, double-chirped waveguide gratings for dispersion compensation and nonlinear Michelson Interferometers for generating an artificial saturable absorber to implement additive pulse mode locking on chip. First results of devices at 1.9 μm using thulium doped aluminum-oxide glass and operating in the Q-switched mode locking regime are presented.

Keywords: integrated optics, integrated mode-locked lasers, silicon photonics, rare-earth mode-locked lasers,

1. INTRODUCTION

Mode-locked lasers providing pico and femtosecond laser pulses are key components of many optical systems such as time-resolved optical pump-probe systems, seeding of optical amplifiers, optical sampling and photonic optical to analog conversion systems [1] and lately optical frequency combs for spectroscopy [2], optical clocks [3], optical signal synthesizers [4] and low noise microwave generation via optical frequency division [5]. Many of these applications ask for miniaturization, i.e. integrated versions of mode-locked lasers on a silicon photonics platform, since they require additional sophisticated optical and electronic sub-systems for spectroscopic analysis, signal processing and analog to digital conversion. Therefore, there is great incentive to realize integrated mode-locked lasers with pulse-widths in the femtosecond range and low noise. III-V gain materials can be brought to bear on a silicon photonics platform via heterogeneous integration [6]. Due to the success of the recently demonstrated planar waveguide lasers utilizing rare-earth doped materials as the gain medium [7],[8] and its co-integration on a silicon-photonics platform through post-processing that involves only single-step deposition of the gain medium on the otherwise completely prefabricated and processed electronic-photonic wafer [9-12], the mode-locked lasers based on rare-earth doped gain media become possible. The advantage is that the gain waveguide is comprised of a glass material where two-photon absorption occurs at much higher peak-intensities compared to III-V materials, and, therefore shorter and more energetic pulses can be directly generated from the mode-locked laser. The higher intracavity pulse energy and shorter pulses enable lower-jitter pulse trains from the laser, which is of key importance for many applications [13].[1]

In section 2, we describe the technology platform in terms of gain media for 1.9 μm and 1.5 μm lasers, i.e. thulium and erbium doped glass gain media and their key parameters, as well as the photonic layer stack chosen. In section 3, we discuss the integrated laser architecture and some of its main components such as the gain waveguide, the pump/signal combiners and transition structures. Section 4 describes the implementation of the on-chip mode locking mechanism that

* currently at MIT Lincoln Laboratory, 244 Wood Street, Lexington, MA 02420

Silicon Photonics: From Fundamental Research to Manufacturing, edited by Roel G. Baets, Peter O'Brien, Laurent Vivien, Proc. of SPIE Vol. 10686, 106860F · © 2018 SPIE
CCC code: 0277-786X/18/$18 · doi: 10.1117/12.2318010

Downloaded From: https://www.spiedigitallibrary.org/conference-proceedings-of-spie on 6/18/2018 Terms of Use: https://www.spiedigitallibrary.org/terms-of-use

has been chosen, which is additive pulse mode locking via a nonlinear Michelson Interferometer that acts as a passive and fast saturable absorber in the mode-locked laser cavity. Section 5 discusses the double-chirped gratings to achieve dispersion compensation in the laser. Finally, in section 6, we present first results for the 1.9 μm wavelength range, demonstrating Q-switched mode-locking, and in the conclusion section, we discuss strategies on how to overcome this instability to eventually achieve a clean cw-mode-locked pulse train with low jitter.

2. TECHNOLOGY PLATFORM

2.1 Rare-Earth-Doped Gain Material

Rare-earth-doped glasses and crystals are amongst the most powerful and technologically important laser materials. For integrated optics applications, the ability to deposit a thin film of amorphous glass via physical vapor deposition provides a significant advantage over crystalline host materials, which require epitaxial growth [10]. Aluminum oxide glass (Al_2O_3) has been extensively studied as a host material for rare-earth ions and has a number of advantageous qualities, chief among them the ability to be deposited at temperatures sufficiently low to be compatible with CMOS electronics fabrication [10]. Here, we concentrate on two specific gain materials, erbium-doped and thulium-doped aluminum oxide, for laser operation at 1550nm and 1900nm respectively. Figure 1 shows the energy level diagrams and transitions relevant for laser operation for both laser materials. Energy transfer upconversion (ETU, see dotted and dashed arrows in Fig.1) can have a deterimental impact on gain, depleting the excited-state laser level and inhibiting population inversion. The impact of these processes in erbium-doped aluminum oxide has been characterized in detail in [9]. In highly-doped thulium fiber lasers and channel waveguides, the cross-relaxation (CR, see dashed arrows in Fig.1) effect has been shown to increase the slope efficiency above 70% [14],[15]. Here, we consider only in-band pumping of thulium at 1600 nm, and thus neglect these ETU and CR processes. Fully three-dimensional gain models for guided modes, incorporating whenever possible, experimentally measured material parameters have been developed to predict achievable modal gain and output power from waveguide amplifiers used in this work [16].

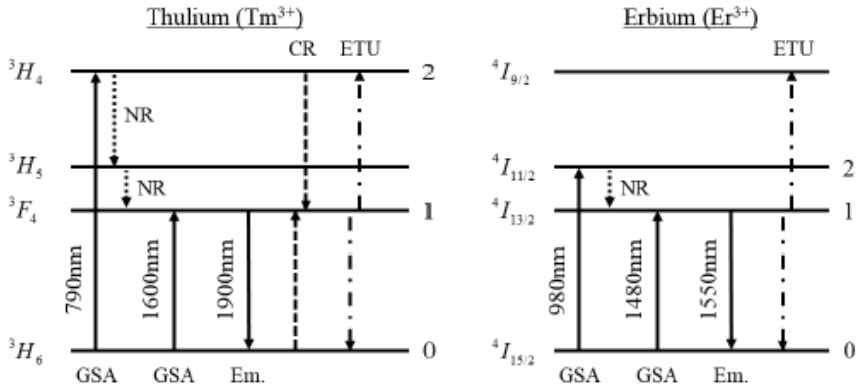

Figure 1. Energy levels and relevant transitions for Thulium (left) and Erbium (right). Abbreviations are as follows: GSA – ground-state absorption, NR – non-radiative transition. Em – emission (spontaneous and stimulated), CR – cross-relaxation, ETU – energy transfer upconversion. The wavelengths of key transitions involved in two- and three-level pumping schemes are labeled [16].

Table 1. Thulium and Erbium gain parameters

Gain Medium	Absorption Cross Section 10^{-21} cm^2	Emission Cross Section 10^{-21} cm^2	Emission Wavelength μm	Upper State Lifetime ms	Effective Mode Area μm^2	Sat. Power mW
Tm: 790 nm pump	6.5 [29]	2.5 [17]	1.9	0.57 [18]	5	2.0
Tm: 1600 nm pump	2.7 [29]	2.5 [17]	1.9	0.57 [18]	5	3.2
Er: 980 nm pump	2.0 [7]	3.7 [7]	1.55	7.5 [7]	5	0.13
Er: 1480 nm pump	3.4 [7]	3.7 [7]	1.55	7.5 [7]	5	0.13

Downloaded From: https://www.spiedigitallibrary.org/conference-proceedings-of-spie on 6/18/2018 Terms of Use: https://www.spiedigitallibrary.org/terms-of-use

Key parameters for thulium and erbium gain media are summarized in Table 1. Thus to achieve in the Thulium waveguide laser pumped at 1600 nm with saturation power of 3.2 mW (see Table 1) , an average intracavity power of about 100 mW, we expect that we need to be able to pump this laser about 30 times over threshold. Judging from the Thulium bandwidth of over 100 nm, we can aim at pulse durations as short as 100 fs, which would result in an intracavity peak power of 1kW.

2.2 Photonic Layer Stack

To ensure compatibility with photonic and electronic sub-systems for advanced applications, the proposed mode-locked lasers are designed for fabrication in a CMOS-compatible silicon-photonics platform at the Colleges of Nanoscale Science and Engineering (CNSE) at the SUNY Polytechnic Institute. The platform consists of three silicon-nitride layers, a silicon layer with eight doping levels, two metal and via layers, a dicing trench for fiber coupling, and a trench for deposition of either an erbium-doped or a thulium-doped aluminum oxide film (performed at MIT). Figure 2 shows a simplified schematic of the layers in this full active platform [16].

As a proof of concept demonstration, the mode-locked lasers demonstrated here are fabricated in a simplified version of the full active platform, which includes three original silicon-nitride layers, the dicing and laser trenches, and a heater metal layer. For these demonstrations, 300-mm-diameter silicon wafers are used with a 6 µm buried oxide thickness. One 400-nm-thick and two 200-nm-thick silicon-nitride layers are deposited using a plasma-enhanced chemical vapor deposition process, polished using a top surface polishing process to reduce optical scattering loss, annealed to reduce absorption, patterned using 193 nm immersion lithography, and processed using a wet oxidation step to reduce side wall roughness [19]. These three layers, called the bottom nitride (BN), first nitride (FN), and second nitride (SN), define the passive devices in the mode-locked laser. Next, a 4-µm-thick silicon-dioxide layer is deposited above the second nitride, a 4-µm-deep trench for deposition of the gain media is etched into the silicon-dioxide using the SN layer as an etch stop, and a 100-nm-thick silicon-dioxide liner is deposited within the laser trench [19]. A deep dicing trench is also etched to define the edge of each chip and enable dicing and edge coupling to fibers. At MIT, a nominally 1100-nm-thick thulium-doped aluminum oxide film is deposited on top of the chip via reactive co-sputtering. The film thickness, deposition temperature, and doping energy are optimized to ensure efficient lasing and proper net intracavity dispersion and may slightly deviate from 1100 nm. Finally, a heater metal layer consisting of 150 nm of titanium and 100 nm of gold is patterned and deposited using a standard photolithography process with lift-off [20].

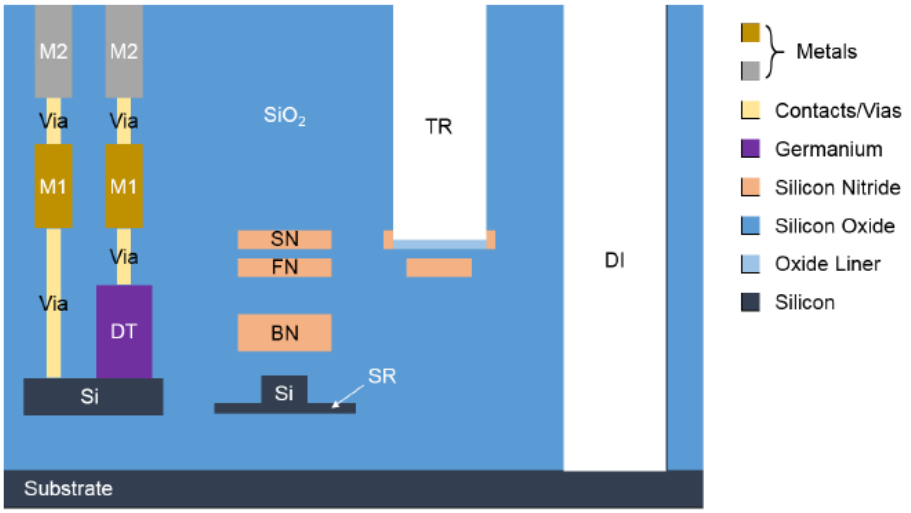

Figure 2. Simplified schematic of the photonic layers in the full active platform: M1 – metal layer 1, M2 – metal layer 2, DT – detector layer, SR – silicon partial-etch ridge, BN – bottom nitride, FN– first nitride, SN – second nitride, TR – photonic trench, DI – dicing trench [16].

Downloaded From: https://www.spiedigitallibrary.org/conference-proceedings-of-spie on 6/18/2018 Terms of Use: https://www.spiedigitallibrary.org/terms-of-use

3. INTEGRATED LASER ARCHITECTURE AND COMPONENTS

3.1 Overall Laser Architecture

The architecture of the integrated mode-locked lasers is shown in Figure 3 with the various intracavity components labeled. First, the input from the pump laser is coupled onto the chip by means of a tapered nitride waveguide, designed to maximize the coupling efficiency from a lensed fiber. The pump is then coupled into the laser cavity with a wavelength combining component, and then into the gain region through several transition components. The gain waveguide is segmented into three separate sections connected by compact bends, in order to increase the total gain length beyond the width of the photonic chip. The total gain length is approximately 6 cm. Dispersion compensation is achieved with an apodized chirped grating, which will be described in a later section. Finally, mode locking is intended to be achieved with a nonlinear interferometer using nitride waveguides, which acts as an artificial saturable absorber. The output from this component is then coupled off chip to serve as the primary laser output port.

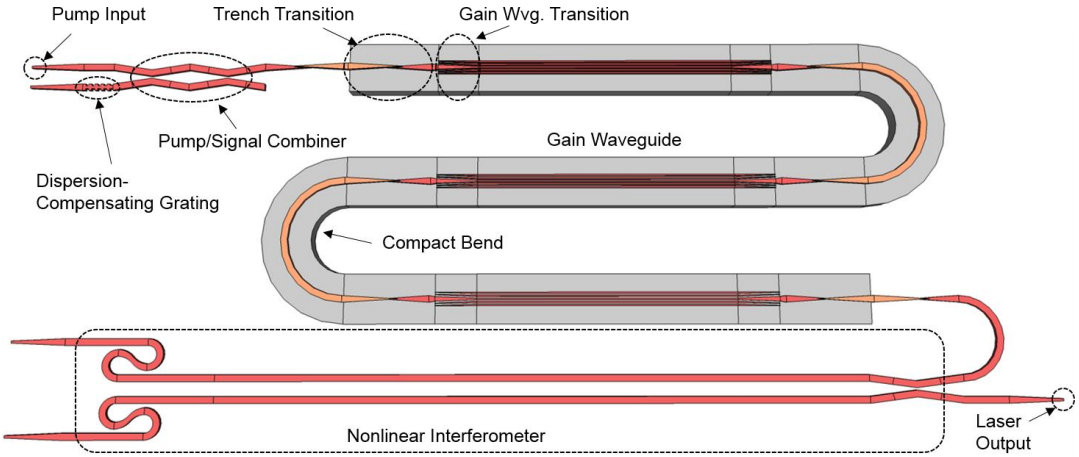

Figure 3. Schematic of the mode-locked laser architecture. Nitride waveguides are shown in red and orange, and the trench region is shown in gray.

3.2 Gain Waveguide

As mentioned before, the gain waveguide is formed by etching a trench into the top silicon dioxide layer, and then depositing a layer of thulium-doped Al_2O_3 on top. A thin layer of silicon nitride beneath the trench provides a guiding material for the optical mode, since the refractive index of Si_3N_4 is higher than the surrounding materials. A buffer layer of SiO_2 reduces the confinement factor in the nitride, and helps to push the mode up into the active material. A diagram of the layer stack is shown in Figure 2. The modal gain is determined by the fraction of the mode in the active material, the degree to which the pump mode adequately inverts the population in the area and the signal and pump mode overlap while maximizing the fraction of the signal mode in the active layer. These goals can be achieved with a diluted Si_3N_4 rib just underneath the gain material as shown in Figure 4 (a). Dilution of the index is achieved by breaking up the Si_3N_4 into 5 pieces. Figures 4 (b) and (c) show the resulting mode profiles for signal and pump wavelength.

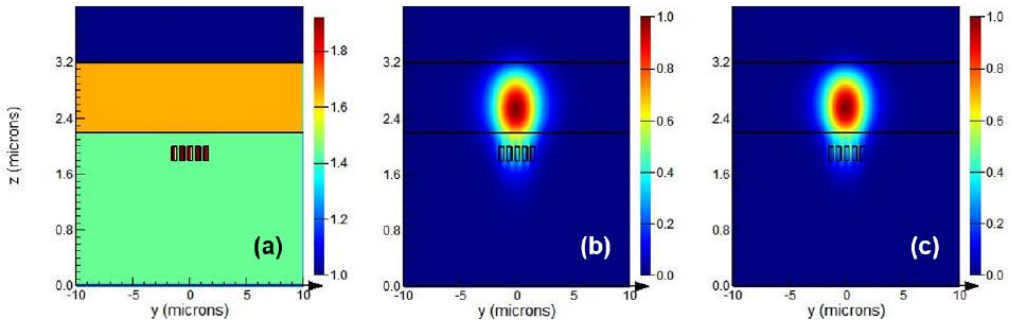

Figure 4. (a) Cross-section of the gain waveguide. Optical intensity distribution at 1900 nm (b) and 1600 nm (c) [16].

Downloaded From: https://www.spiedigitallibrary.org/conference-proceedings-of-spie on 6/18/2018 Terms of Use: https://www.spiedigitallibrary.org/terms-of-use

The confinement factors of the signal and pump modes in the gain material is about 80% and the mode overlap between the pump and signal modes in the gain region is 60%.

3.3 Pump/Signal Combiner and Transition Structures

To couple the pump light into the laser cavity without incurring excess loss by pumping through the grating, we designed a Mach-Zehnder-based pump/signal combiner. The device is comprised of two integrated directional couplers back-to-back, which is essentially a Mach-Zehnder interferometer with zero phase difference between the two arms, as shown in Figure 5. We designed the directional coupler to have a 50/50 splitting ratio at the signal wavelength, and minimal coupling at the pump wavelength. Therefore, the incoming pump light is coupled through from port 2 to port 4, and the signal light is coupled across from port 1 to port 4. The extinction ratio at the pump wavelength was measured to be 16dB, which corresponds to an excess loss of 0.1 dB from port 2 to port 4. The excess loss at the signal wavelength from port 1 to port 4 was measured to be 0.6 dB.

Figure 5. Schematic of pump/signal combiner.

Once the pump and signal paths are combined, light is then coupled into the gain waveguide by means of a series of adiabatic transition structures. The gain region is defined by the trench, mentioned previously, which is etched into the top SiO_2 layer and partially filled by the Tm^{3+}:Al_2O_3 film. Therefore, to couple light efficiently across the boundary of the trench requires that the optical mode be confined in a nitride waveguide, this is in fact the purpose of introducing the thicker bottom nitride (BN) layer into the photonic stack. The thickness of the BN layer was chosen to be 400 µm, and the spacing between the BN layer and the FN layer was chosen to be 450µm, such that the loss is minimal when crossing the trench boundary. Once the BN waveguide has crossed the trench boundary, the optical mode must be drawn up into the gain material in order to transition into the gain waveguide. This is accomplished by first tapering up an FN waveguide above the BN layer, then tapering down the BN waveguide such that the mode is adiabatically shifted vertically upwards into the FN layer. The length of the transition is chosen to be 350 µm to ensure that the taper is adiabatic. The insertion loss of this component was measured at 1900 nm using the cutback method, the results (after calibrating out the coupling losses in the measurement) are shown in Figure 6.

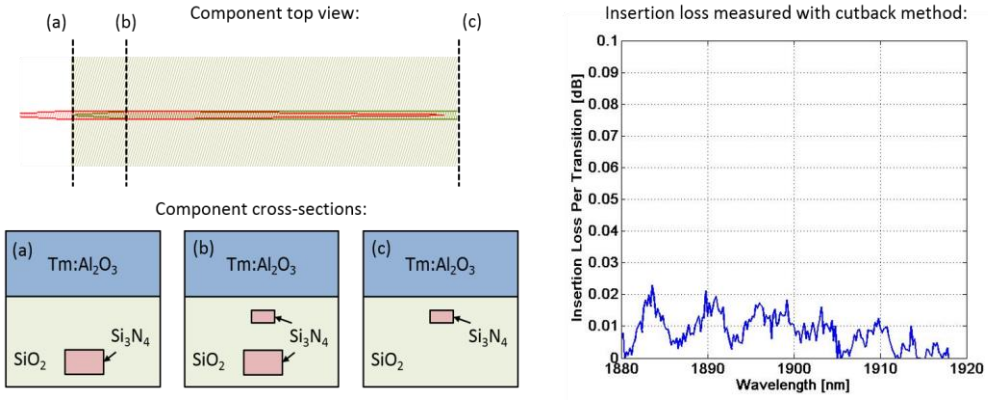

Figure 6. (Left) Top-view schematic of trench transition component with cross-sections at various positions. (Right) Measured insertion loss per transition, at the signal wavelength, after coupling loss calibration [16].

After the transition into the trench region, another transition is required to transform the waveguide cross-section from a single nitride piece to the five-piece segmented nitride gain waveguide described earlier. This is achieved with a simple linear taper, in which the nitride pieces on either side of the central piece are tapered up in width, while the width of the central piece is tapered down, as shown in Figure 7. The insertion loss at 1900 nm was measured to be ~0.02dB per transition using the cutback method.

Downloaded From: https://www.spiedigitallibrary.org/conference-proceedings-of-spie on 6/18/2018 Terms of Use: https://www.spiedigitallibrary.org/terms-of-use

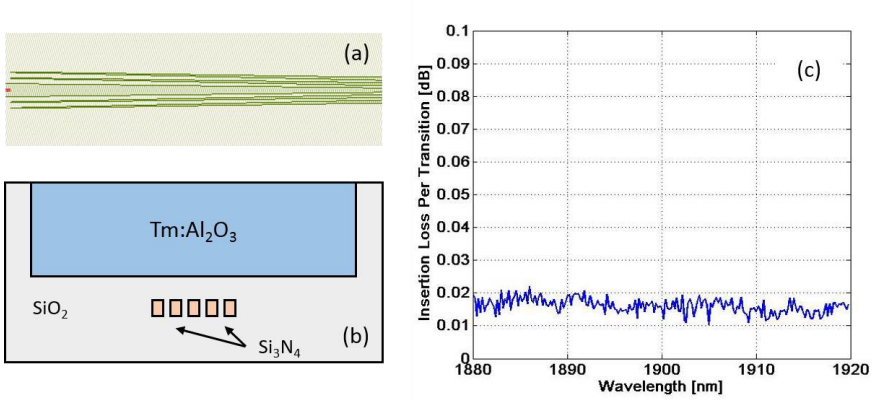

Figure 7. (a) Top-view schematic, (b) cross-section, and (c) measured insertion loss of the gain waveguide transition [16].

4. ADDITIVE PULSE MODELOCKING WITH A NONLINEAR MICHELSON INTERFEROMETER

Additive pulse mode locking using the Kerr-nonlinearity in fibers or in external cavities to create an artificial saturable absorber for mode locking of lasers has been studied extensively in the area of solid-state and fiber lasers [21],[22]. The idea is to use the Kerr-effect-induced self-phase modulation on a pulse when propagating through a waveguide or fiber and convert it into a self-amplitude modulation via an interferometric device [22]. Here, we implemented a nonlinear Michelson Interferometer with high contrast Si_3N_4 waveguides, as shown in Fig. 8. The interferometer arms are ended with loop mirrors enabling broadband high reflection of about 98% on-chip. The arm length can be as long as the reticle length of 2.4 cm to maximize the nonlinear phase shift for a given peak power.

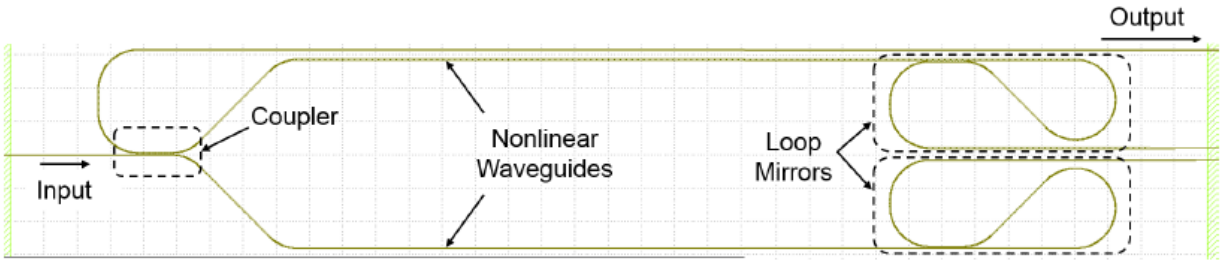

Figure 8. Mask layout of a nonlinear Michelson Interferometer test structure, with constituent sub-components labeled. Device as shown is not to scale [20],[23].

The nonlinear transmission characteristics from input to output of the nonlinear Michelson Interferometer has been measured with an OPO with 80 MHz repetition rate producing 200 fs pulses tuned to 1900 nm. Figure 9 shows the measurement results as a function of input peak power after calibrating and subtracting out the on-chip coupling losses.

Clearly, the structure proves around 10% of intensity dependent transmission and, therefore, also reflection modulation equivalent to a fast saturable absorber within the linear laser cavity, when properly biased with a heater.

Downloaded From: https://www.spiedigitallibrary.org/conference-proceedings-of-spie on 6/18/2018 Terms of Use: https://www.spiedigitallibrary.org/terms-of-use

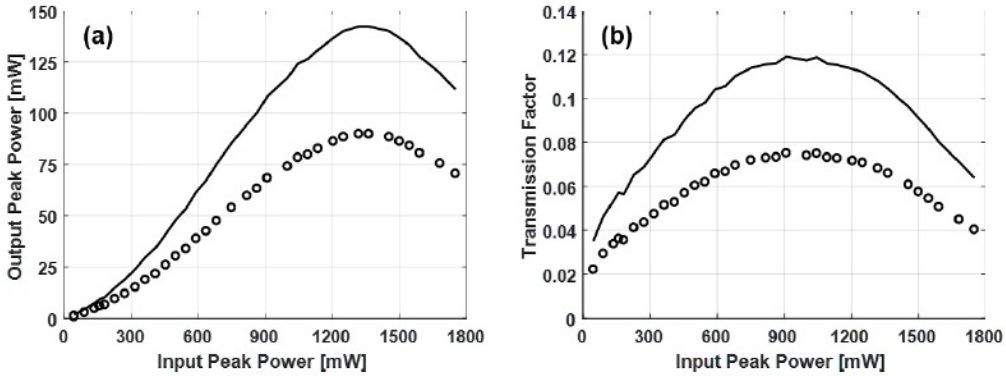

Figure 9. Measured response of the nonlinear Michelson Interferometer test structure. (a) Output peak power as a function of input peak power. (b) Transmission P_{out}/P_{in} as a function of input peak power. Black circles denote the measured data at the edge of the chip, after coupling loss calibration. Solid lines correspond to corrected data, after factoring out the output waveguide loss of the test structure [20],[23].

5. DISPERSION COMPENSATING GRATINGS

Chirped fiber Bragg gratings are now widely deployed for stretching and compression of optical pulses in fiber and are extensively used for dispersion compensation in fiber lasers. Its theoretical description using coupled-mode theory is well developed [25]. Therefore, it is natural here to use waveguide gratings, see Figure 10, to achieve proper dispersion compensation in the mode-locked waveguide lasers to enable stable pulse formation in the presence of strong self-phase modulation due to the desired high peak power. To achieve a smooth group delay dispersion we implemented an adiabatic apodization of the grating at both ends of the waveguide by bringing the grating sections in slowly from the side to the main waveguide and departing it at the end of the waveguide section to avoid spurious reflections both at the beginning and end of the grating, see Figure 11. Over the waveguide length, the Bragg wavelength of the grating is chirped over the desired wavelength range to provide both high reflectivity as well as a desired dispersion over that wavelength range. The dispersion and reflectivity values achievable are determined by the length and modulation depth of the grating as well as the slope in chirp of the Bragg wavelength over the length of the grating.

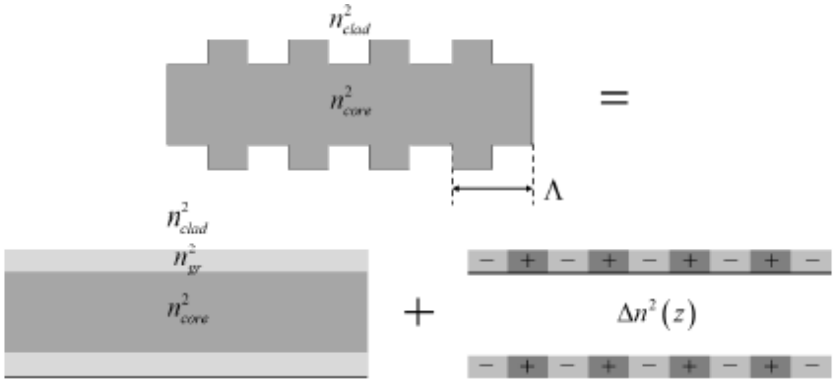

Figure 10. Illustration of the Bragg grating implemented as a corrugated waveguide. The structure can be decomposed into the sum of a z-invariant reference waveguide, with some intermediate refractive index n_{gr} between the core and the cladding, and a periodic index perturbation $\Delta n(z)$.

We have designed both gratings in the thinner FN- Si_3N_4 – layer as well as the thicker BN-Si_3N_4 – layer. Due to the increased thickness of the BN-layer a stronger index grating is possible making these type of gratings more broadband, but in general less dispersive. Figure 12 shows the designed characteristics of the broadband gratings. The devices show a flat group delay dispersion (GDD) profile across the entire gain band of thulium, in order to support the formation of ultrashort pulses within the laser cavity. The width of the central BN waveguide was 900 nm and the width of the

Downloaded From: https://www.spiedigitallibrary.org/conference-proceedings-of-spie on 6/18/2018 Terms of Use: https://www.spiedigitallibrary.org/terms-of-use

perturbation blocks was 1.6 μm. Each of the four devices are simulated to have > 80% reflection over a 100-nm bandwidth centered at 1900 nm, with the longer devices anticipated to deliver > 90% reflection over that same wavelength range. The bandwidth coverage of the grating of about 100 nm would be broadband enough to support sub-100 fs pulses at 1.9 μm.

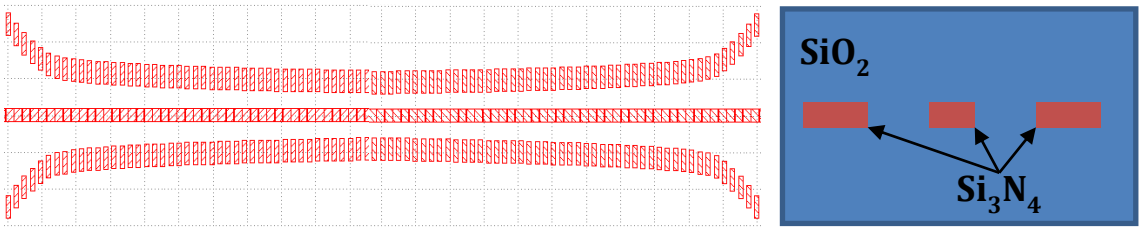

Figure 11. Top view of mask layout for a double-chirped grating where the coupling is adiabatically switched on by bringing the grating sections slowly closer to the main waveguide where the guided light comes in [16].

Similar gratings have been fabricated at 1550 nm and carefully characterized showing excellent agreement between designed and measured dispersion and reflection characteristics.

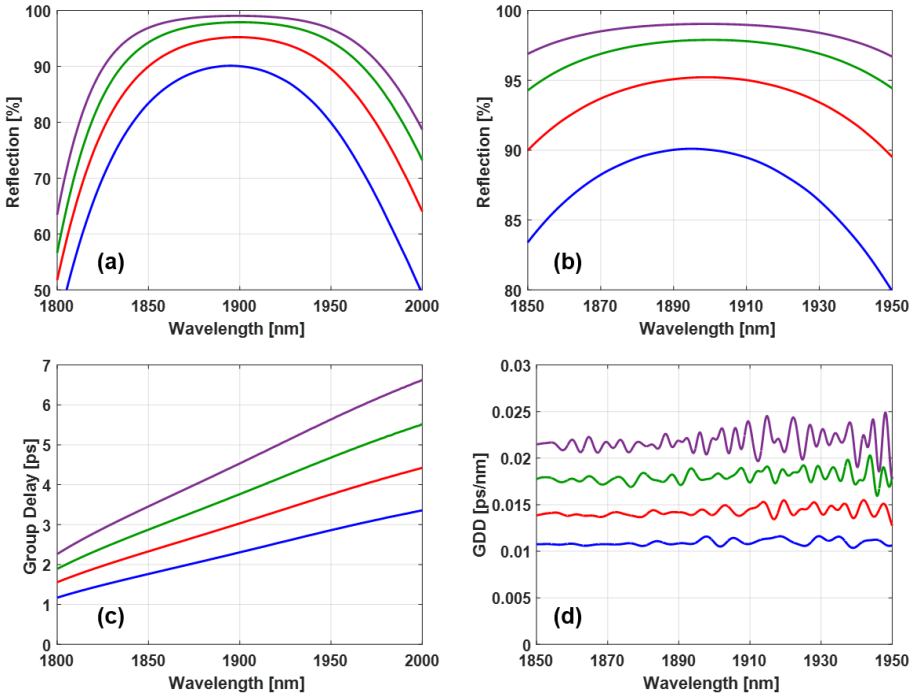

Figure 12. Simulated performance of four BN double-chirped grating designs with different target dispersion values. (a,c) Reflectivity and group delay over the wavelength range of interest. (b,d) Reflectivity and GDD over the wavelength range of interest [16].

6. EXPERIMENTAL RESULTS

Here, we discuss first results achieved with the 1.9 μm laser structure. Figure 13(a) shows the optical spectrum of the mode-locked laser corresponding to 350 mW of on-chip pump power and 4 mW signal output power from a 10% output coupler. Thus the intracavity power is about 40 mW. The broad spectrum indicates short pulse formation. The 3dB

Downloaded From: https://www.spiedigitallibrary.org/conference-proceedings-of-spie on 6/18/2018 Terms of Use: https://www.spiedigitallibrary.org/terms-of-use

bandwidth of the spectrum is 17 nm, corresponding to 215 fs transform-limited pulses. The corresponding RF spectrum is shown in Figure 13(b) with a 1.2 GHz mode spacing, corresponding to ~13cm round-trip mode-locked laser cavity length. Figure 13(c) shows that the time-domain data correspond to a train of mode-locked pulses modulated with a Q-switching envelope of 720 kHz repetition rate. The duration of the Q-switching envelope is about one tenth of the Q-switching period, i.e. 100 ns. Figure 13(d) shows a close-up of one Q-switched pulse, where under the Q-switching envelope, individual cw-mode-locked pulses are visible with 0.8 ns spacing, corresponding to the 1.2 GHz fundamental repetition rate of the mode-locked laser.

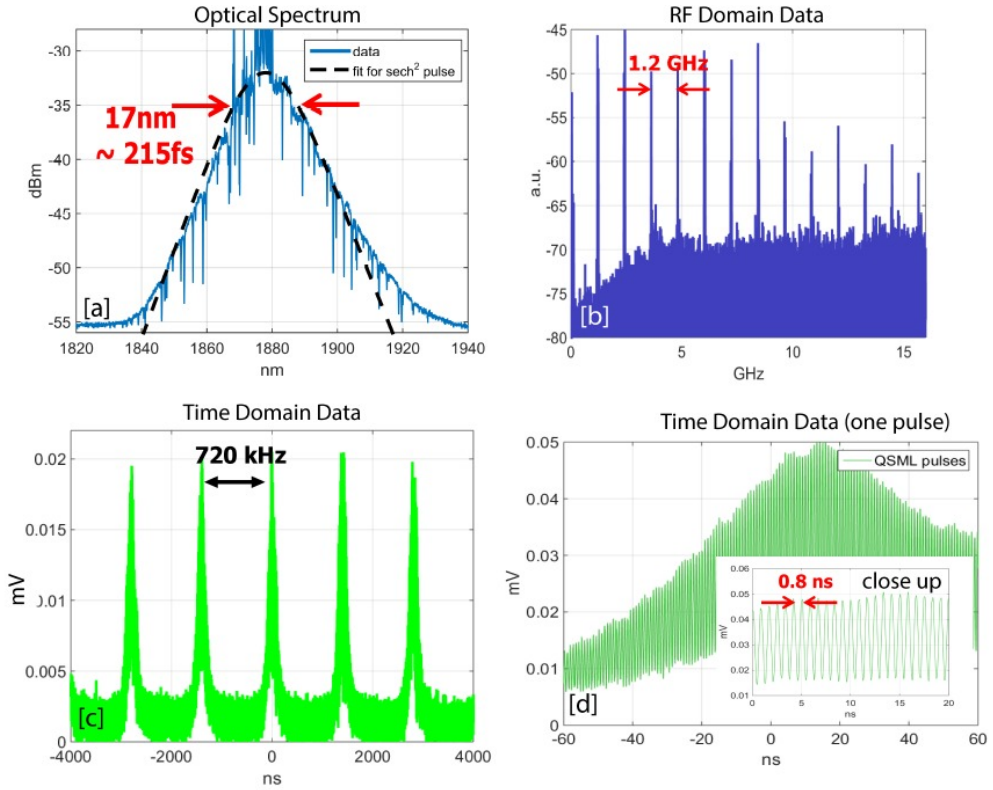

Figure 13. Experimental results for devices operating currently in the Q-switched mode locking regime. (a) Optical spectrum of the mode-locked laser structure shown in Figure 3; (b) RF spectrum of the mode-locked laser; (c) Time-domain data showing the Q-switching cycle with about 1.4 μs period; (d) Close-up of time-domain signal showing Q-switched mode-locking [20],[24].

7. CONCLUSION

We have described a mode-locking architecture and components of a fully integrated mode-locked laser on a silicon photonics platform based on rare-earth doped gain media. Results with first devices at 1.9 μm lead to Q-switched mode-locked operation producing 4 mW of output power of potentially 217 fs pulses at 1.2 GHz repetition rate. Current work is geared towards full characterization of the pulse duration and suppression of the Q-switching instability. Q-switched mode-locking is often observed in mode-locked lasers, when the peak power of the pulse train can not yet saturate the saturable absorption that forms the ultrashort pulses but also initiates Q-switching. Efficient strategies for suppression of Q-switched mode locking include either feedback stabilization of intracavity power via an intracavity loss modulator or feedback stabilization of gain via pump modulation and/or further optimization of intracavity pulse parameters and pulse shaping. Together with the other components developed on the same silicon photonics platform, such as octave-spanning continuum generation [27] and on-chip second harmonic generation via an electric-field-induced second-order nonlinearity (EFISH) in silicon [28], these lasers would enable frequency comb generation and optical frequency synthesis on a complete silicon photonics platform.

Downloaded From: https://www.spiedigitallibrary.org/conference-proceedings-of-spie on 6/18/2018 Terms of Use: https://www.spiedigitallibrary.org/terms-of-use

8. ACKNOWLEDGEMENT

This work was supported by the Defense Advanced Research Projects Agency (DARPA) under the DODOS project (grant no. HR0011-15-C-0056). The authors thank J. D. B. Bradley, G. Riggott and K. Broderick for discussions and assistance on thin film deposition. N. Li acknowledges a fellowship from the Agency of Science, Technology and Research (A*STAR), Singapore. K. Shtyrkova acknowledges National Defense Science and Engineering Graduate Fellowship (32 CFR 168a).

REFERENCES

[1] A. Khilo, S. J. Spector, M. E. Grein, A. H. Nejadmalayeri, Ch. W. Holzwarth, M. Y. Sander, M. S. Dahlem, M. Y. Peng, M. W. Geis, N. A. DiLello, J. U. Yoon, A. Motamedi, J. S. Orcutt, J. P. Wang, Ch. M. Sorace-Agaskar, M.A. Popović, J. Sun, G. R. Zhou, H. Byun, J. Chen, J. L. Hoyt, H. I. Smith, R. J. Ram, M. Perrott, Th. M. Lyszczarz, E. P. Ippen, and F. X. Kärtner, "Photonic ADC: overcoming the bottleneck of electronic jitter," Opt. Express **20**(4) 4454-4469 (2012).

[2] S. Diddams, "The evolving optical frequency comb," J. of the Opt. Soc. of America B **27**, 51-62 (2010).

[3] S. B. Papp, K. Bea, P. Del Haye, F. Quinlan, H. Lee, K. Vahala and S. Diddams, "Microresonator frequency comb optical clock," Optica **1**, 10-14 (2014).

[4] T. R. Schibli, K. Minoshima, F.-L. Hong, H. Inaba, Y. Bitou, A. Onae, H. Matsumoto, "Phase-locked widely tunable optical single-frequency generator based on a femtosecond comb," Opt. Lett. **30**, 2323-5 (2005).

[5] T. M. Fortier, M. S. Kirchner, F. Quinlan, J. Taylor, J. Bergquist, T. Rosenband, N. Lemke, A. Ludlow, Y. Jiang, C. Oates, et al., "Generation of ultrastable microwaves via optical frequency division," Nat. Photonics **5** (7), 425 (2011).

[6] M. Davenport, J. Bowers and S. Liu, "Integrated Heterogeneous Silicon/III-V Mode-Locked Lasers," to appear in Photonics Research.

[7] J. D. Bradley, "$Al_2O_3:Er^{3+}$ as a gain platform for integrated optics", PhD thesis, University of Twente, 2009.

[8] J. D. Bradley and M. Pollnau, "Erbium-doped integrated waveguide amplifiers and lasers," Laser & Photonics Reviews **5**(3), 368–403 (2011).

[9] Purnawirnam, J. Sun, T. N. Adam, G. Leake, D. Coolbaugh, J. D. B. Bradley, E. S. Hosseini, and M. R. Watts, "C- and L- Band erbium-doped waveguide lasers with wafer-scale silicon nitride cavities," Opt. Lett. **38**(11), 1760-1762 (2013).

[10] E. S. Magden, N. Li, Purnawirman, J. D. B. Bradley, N. Singh, A. Ruocco, G. S. Petrich, G. Leake, D. D. Coolbaugh, E. P. Ippen, M. R. Watts, and L. A. Kolodziejski, "Monolithically-integrated distributed feedback laser compatible with CMOS processing," Opt. Express **25**(15), 18058–18065 (2017).

[11] N. Li, Purnawirman, Z. Su, E. Salih Magden, P. T. Callahan, K. Shtyrkova, M. Xin, A. Ruocco, C. Baiocco, E. P. Ippen, F. X. Kärtner, J. D. B. Bradley, D. Vermeulen, and M. R. Watts, "High-power thulium lasers on a silicon photonics platform," Opt. Lett. **42**(6), 1181-1184 (2017).

[12] C. M. Sorace-Agaskar, P. T. Callahan, K. Shtyrkova, A. Baldycheva, M. Moresco, J. Bradley, M. Y. Peng, N. Li, E. S. Magden, Purnawirman, M. Sander, G. Leake, D. Coolbaugh, M. R. Watts, F. X. Kärtner "Integrated mode-locked lasers in a CMOS-compatible silicon photonic platform," in *CLEO: Science and Innovations*, 2015, p. SM2I. 5.

[13] J. Kim and F. X. Kärtner, "Attosecond Precision Ultrafast Photonics," Laser & Photon. Rev. **4**(3), 432-456 (2010).

[14] J. Wu, Z. Yao, J. Zong, and S. Jiang, "Highly efficient high-power thulium-doped germinate glass fiber laser," Opt. Lett. **32**(6), 638–640 (2007).

[15] K. van Dalfsen, S. Aravazhi, C. Grivas, S. M. García-Blanco, and M. Pollnau, "Thulium channel waveguide laser with 1.6 W of output power and 80% slope efficiency," Opt. Lett. **39**(15), 4380–4383 (2014).

[16] P. T. Callahan, "Integrated Waveguide Devices for Mode-Locked Lasers," PhD thesis, MIT, 2018.

[17] P. Loiko and M. Pollnau, "Stochastic model of energy-transfer processes among rare-earth ions. Example of Al2O3:Tm3+," J. Phys. Chem. C, **120**(46), 26480-26489 (2016).

Downloaded From: https://www.spiedigitallibrary.org/conference-proceedings-of-spie on 6/18/2018 Terms of Use: https://www.spiedigitallibrary.org/terms-of-use

[18] E. Magden, P. Callahan, N. Li, J. Bradley, N. Singh, A. Ruocco, L. Kolodziejski, E.P. Ippen, and M.R. Watts, "Frequency domain spectroscopy in rare-earth-doped gain media," IEEE J. Sel. Topics in Quantum Electron. **24**(5), 1-10 (2018).
[19] J. D. Bradley, E. S. Hosseini, Purnawirman, Z. Su, T. N. Adam, G. Leake, D. Coolbaugh, and M. R. Watts**,** **"**Monolithic erbium- and ytterbium doped microring lasers on silicon chips," Opt. Express **22**, 12226-12237 (2014).
[20] K. Shtyrkova, "Fully Integrated CMOS-Compatible Mode-Locked Lasers," PhD thesis, MIT, 2017.
[21] H. A. Haus, J. G. Fujimoto, E. P. Ippen, "Structures for additive pulse modelocking," J. of the Opt. Soc. Am. B **8**, 2068-2076 (1991).
[22] H. A. Haus, J. G. Fujimoto, E. P. Ippen, "Analytic Theory of Additive Pulse and Kerr Lens Mode Locking," IEEE J. Quantum Electron. **28**, 2086-2096 (1992).
[23] K. Shtyrkova, P. T. Callahan, E. P. Ippen, F. X. Kärtner, "Fully-integrated artificial saturable absorber based on Kerr nonlinearity in silicon nitride," *CLEO 2017*, Paper AF1B.6, San Jose, CA, USA, 2017.
[24] K. Shtyrkova, P. T. Callahan, N. Li, E. S. Madgen, M. R. Watts, F. X. Kartner, and E. P. Ippen, "Integrated CMOS-compatible Q-Switched-Mode-Locked Laser at 1.9μm with On-Chip Artificial Saturable Absorber", in *Advanced Photonics 2018*, paper IM3B.2, OSA
[25] K. O. Hill and G. Meltz, "Fiber Bragg grating technology fundamentals", Opt. Lett. **18**, 953–955 (1993).
[26] P. T. Callahan, K. Shtyrkova, N. Li, E. S. Magden, C. Baiocco, D. Coolbaugh, E. P. Ippen, M. R. Watts, and F. X. Kärtner, "Fully-Integrated CMOS-Compatible Q-Switched Laser at 1.9μm Using Thulium-Doped Al2O3" *CLEO 2017*, Paper STh3N.2, San Jose, CA, USA, 2017.
[27] N. Singh, M. Xin, D. Vermeulen, K. Shtyrkova, N. Li, P. T. Callahan, E. S. Magden, A. Ruocco, N. Fahrenkopf, C. Baiocco, B. P. P. Kuo, S. Radic, E. Ippen, F. X. Kärtner, and M. R. Watts, "Octave-spanning coherent supercontinuum generation in silicon on insulator from 1.06 μm to beyond 2.4 μm," Light: Science & Applications **7**, 17131 (2018).
[28] E. Timurdogan, C. V. Poulton, M. J. Byrd, and M. R. Watts, "Electric field-induced second-order nonlinear optical effects in silicon waveguides" Nature Photonics **11**, 200–206 (2017).
[29] E. S. Magden, "Optical Signal Generation, Stabilization, and Manipulation in Broadband Silicon Photonics," PhD thesis, MIT, 2017.

Downloaded From: https://www.spiedigitallibrary.org/conference-proceedings-of-spie on 6/18/2018 Terms of Use: https://www.spiedigitallibrary.org/terms-of-use